Monte Carlo Simulations of Polymer Network Deformation

Nisha Gilra,[†] Athanassios Z. Panagiotopoulos,*[,‡,§] and Claude Cohen[†]

School of Chemical Engineering, Cornell University, Ithaca, New York 14853, and Institute for Physical Science and Technology and Department of Chemical Engineering, University of Maryland, College Park, Maryland 20742

Received December 22, 2000; Revised Manuscript Received April 4, 2001

ABSTRACT: The deformation of end-linked polymer networks was investigated by Monte Carlo simulations using the three-dimensional bond fluctuation model. A novel methodology is presented for constant pressure simulations on a lattice that is based on placing a sample between walls. Uniaxial expansion or contraction is performed in a number of intermediate steps by adjusting the wall−polymer potential. The network $P-V$ behavior is found to be similar to the athermal linear chain $P-V$ behavior at high volume fractions, but the network data deviate from that of the linear chains at low volume fractions. At large deformations, elastic chain dimensions are non-Gaussian in the direction of deformation, while remaining approximately Gaussian in directions perpendicular to deformation. Also, the chain segment orientation of the elastic chains in the network and linear probe chains that are trapped in undeformed and deformed networks was determined. The results suggest that segments near the ends of elastic chains in the network deform to greater extents than the chain segments in the center of the chains.

1. Introduction

An unusual and important property of polymer networks is their rubberlike elasticity. Polymer networks have the ability to be deformed to great extents and then elastically spring back to their original form.[1] Due to these properties, elastomeric materials have long been of great interest both technologically and scientifically.

Network deformation, such as swelling in a solvent or uniaxial extension, can be readily performed in the laboratory. From such experiments, macroscopic properties such as equilibrium swelling ratios, elastic moduli, and stress−strain behavior can be determined. These macroscopic properties, however, depend strongly on the microscopic structure of the network. Microscopic properties cannot be determined as easily using experiments.

One area of research in the study of uniaxially deformed networks is chain segment orientation because it may provide information important for understanding rubber elasticity.[2] The chain segment orientation of network elastic chains and free linear probe chains dissolved in a network have been studied experimentally using nuclear magnetic resonance (NMR).[2−8] These studies report that uniaxial deformation of the network induces uniaxial orientation order in segments of the elastic and/or probe chains in the direction of strain. Boué et al.,[9] however, did not observe any indication of segment orientation in a small-angle neutron scattering (SANS) study of trapped linear polymer chains in a strained network. They speculated that the probe chain segment alignment may be occurring at small length scales (detected only by NMR) and not at larger ones. Computer simulations have also been used to study the chain segment orientation of network elastic chains and free linear probe chains in a network, and these studies report similar results as the experimental NMR studies mentioned above.[10−15] We are not aware, however, of any computer simulation studies that have been performed to test the validity of the suggestion of Boué et al. One way of measuring the segment alignment of an elastic chain or a linear probe chain using computer simulations is to determine the orientation correlation between segments of the chains with respect to other segments within the same chain. Determination of the intrachain orientation of chain segments in a deformed network may provide more insight into the NMR and SANS observations.

There are some characteristics of polymer networks that make them difficult to simulate. Real rubberlike materials relax slowly relative to time scales accessible by molecular simulations. One of the major causes of this sluggishness is their cross-link constraints.[16] In fact, the slow relaxation times of networks have prevented continuous, dynamical simulations of deformation. However, alternate techniques have been devised to circumvent the naturally slow relaxation times of polymer networks. Researchers have created models in which the chain ends of a polymer melt are immobilized, and "network" deformation occurs by changing the end-to-end distances in an affine manner[13,16] or by biasing monomer motion such that extended configurations are preferred.[15] Additionally, isotropic swelling of polymer networks has been studied using constant NVT simulations[17,18] where the network is swollen with empty lattice sites that represent the solvent by placing the network in larger and larger lattices. One of these studies was extended by examining the stress−strain behavior of networks using constant NVT simulations in which the deformation process was split up into a series of discrete steps.[19] In another study on swelling,[20] isotropic volume change moves were performed by varying the bond length between monomers. Also, simulations of swelling were performed using the constant NpT ensemble that more closely models experimental conditions but used nonphysical moves involving removal and construction of a slab of material to change the volume.[21−23]

[†] Cornell University.
[‡] University of Maryland.
[§] Current address: Department of Chemical Engineering, Princeton University, Princeton, NJ 08544.

10.1021/ma0021895 CCC: $20.00
Published on Web 07/20/2001

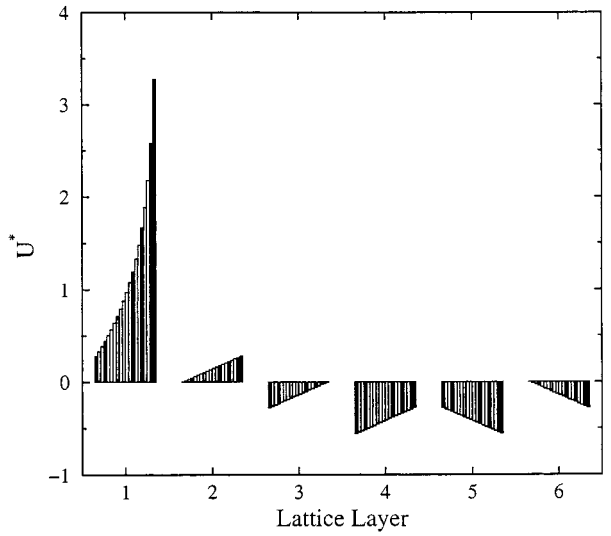

Figure 1. A representation of a 20-step, 7-layer wall−polymer potential used to perform volume change moves for the polymer network systems. The infinite potential at lattice layer 0 is not shown. Each separate bar within a lattice layer represents a step.

The goal of this work is to investigate network deformation using physically realistic volume change moves. Deformations are performed in a constant pressure environment so that the inherent dynamics of the network present during deformation are maintained. This study was performed using constant *NpT* Monte Carlo simulations of polymer networks on a three-dimensional simple cubic lattice using the bond fluctuation model (BFM).[24,25]

For lattice systems, pressure is a difficult variable to hold constant because it requires volume fluctuations of the system that often have low acceptance probabilities. Several methodologies[26−29] have been proposed to perform volume change moves on a lattice but have only been applied to the study of single particles or uncross-linked polymer chains. A new method to perform constant *NpT* simulations on a lattice is proposed here and applied to the study of uniaxial swelling and deswelling of polymer networks.

2. Simulation Methodology and Theoretical Calculations

2.1. Volume Change Move. Deformation of the polymeric systems was performed by placing the sample between two parallel walls that were allowed to move. These simulations were performed using the isothermal−isobaric (constant *NpT*) ensemble, so that the distance between the two walls was allowed to fluctuate in the *z* direction. The linear polymer and polymer network systems were studied with periodic boundaries in the *x* and *y* directions.

Since we are interested in extension as well as compression of polymer samples, the wall−polymer potential must have an attractive component to ensure that the polymer chains adhere to the walls. A key idea in this work is to design a wall potential that can be varied gradually to decrease or increase the effective volume of the simulation box. An example of such a potential is shown in Figure 1. The potential extends over seven lattice layers and is translated by a whole lattice layer in 20 intermediate steps.

The layers are numbered such that there is an infinite potential in layer 0 (which is not shown), so there are no segments present there. The potential in layers 1 and 2 is repulsive and gradually decreasing, so that some chain segments can exist in these layers. Layers 3−6 have an attractive potential to "anchor" the polymer sample during deformation, and from layer 7 and beyond the wall−polymer potential is zero. In principle, a volume change move can be attempted that moves the wall one full lattice position. Such a move, however, is unlikely to have a high probability of acceptance. To allow for volume changes with reasonable acceptance, the volume change move is implemented in a number of partial steps. An example of 20 such steps are shown in Figure 1. Each bar within a lattice layer represents a step. An entire lattice layer is added or removed only when an entire cycle of steps is completed. When the potential is in mid-cycle, the effective volume is calculated as a sum of the Boltzmann factors of the potential over all lattice layers. This approach allows for the calculation of a continuous effective volume that interpolates between effective volumes of individual lattice layers and is similar to the method presented by Pendzig et al.[26] This particular potential was devised so that it is continuous over all layers and allows for reasonable acceptance of attempted volume change moves.

As a consistency check for using this approach, conformational properties of elastic chains in networks were determined using constant *NpT* simulations of networks swollen to equilibrium ($\pi^* = 0$). These properties were also computed using constant *NVT* simulations by allowing the networks to swell to equilibrium on lattices that had increasingly larger lengths in the *z* direction. The properties of both sets of simulations were found to be in excellent agreement.

If it is not necessary to anchor the polymer sample to the wall, a purely repulsive two-layer potential can be used. An example of such a potential is one where the first layer is infinitely repulsive, i.e., $U^*(0,s') = \infty$ for all step numbers s', and the second layer has a potential given by[26]

$$U^*(1,s') = -\ln \frac{s'}{S} \tag{1}$$

where S is the total number of steps in the potential. The value of S dictates the maximum value of the wall−polymer potential, such that $U^*_{max} = \ln S$.

Several properties of interest in the study of deformed networks include the relationship between macroscopic and microscopic deformation ratios and chain segment alignment. The methodology for calculating these properties is discussed below.

2.2. Calculation of the Deformation Ratio. Under deformation, the components of the end-to-end distance of the elastic chains may be expressed as

$$\langle R_{e,x}^2 \rangle = \lambda_x^2 \langle R_{e,x}^2 \rangle_0, \quad \langle R_{e,y}^2 \rangle = \lambda_y^2 \langle R_{e,y}^2 \rangle_0, \quad \langle R_{e,z}^2 \rangle = \lambda_z^2 \langle R_{e,z}^2 \rangle_0 \tag{2}$$

where λ_i is the microscopic deformation ratio in the $i = x$, y, or z direction and the subscript zero denotes the undeformed state. For the affine model, when the network is swollen by a solvent, $\lambda_x\lambda_y\lambda_z = 1/\phi_2$, where $\phi_2 = \phi/\phi_0$ in which ϕ is the volume fraction of the deformed network and ϕ_0 is the volume fraction of the network

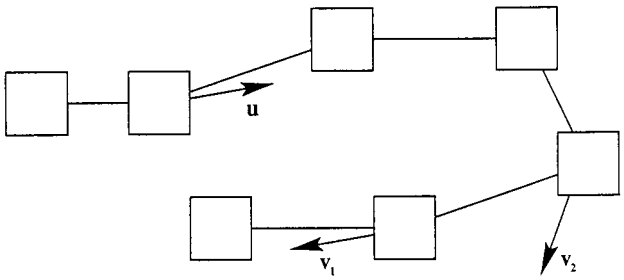

Figure 2. A two-dimensional representation of a 7-mer with vectors **u** and **v** used to demonstrate the method for calculating the orientation correlation, $S(r)$. Two examples of **v** ($\mathbf{v_1}$ and $\mathbf{v_2}$) are shown to illustrate how **v** changes along the contour of the polymer.

at formation. Additionally, for uniaxial deformation or swelling in the z direction, $\lambda_x = \lambda_y$. Combination of these relations with eq 2 leads to

$$\langle R_{e,x}^2\rangle = \frac{\langle R_{e,x}^2\rangle_0}{\lambda_z\phi_2}, \quad \langle R_{e,y}^2\rangle = \frac{\langle R_{e,y}^2\rangle_0}{\lambda_z\phi_2}, \quad \langle R_{e,z}^2\rangle = \lambda_z^2\langle R_{e,z}^2\rangle_0 \tag{3}$$

Furthermore, in the unperturbed state of an isotropic network

$$\langle R_{e,x}^2\rangle_0 = \langle R_{e,y}^2\rangle_0 = \langle R_{e,z}^2\rangle_0 = \langle R_e^2\rangle_0/3 \tag{4}$$

Combination of eqs 3 and 4 leads to a microscopic deformation ratio that is given by

$$\lambda_{z,m1} = \left[\frac{2\langle R_{e,z}^2\rangle}{\phi_2(\langle R_{e,x}^2\rangle + \langle R_{e,y}^2\rangle)}\right]^{1/3} \tag{5}$$

for an affine deformation. This expression can then be compared to the actual microscopic deformation ratio as defined in eq 2

$$\lambda_{z,m2} = \left[\frac{\langle R_{e,z}^2\rangle}{\langle R_{e,z}^2\rangle_0}\right]^{1/2} \tag{6}$$

Finally, the macroscopic value of the deformation ratio can be determined from the dimensions of the network sample before ($L_{z,0}$) and after (L_z) deformation using

$$\lambda_{z,M} = \frac{L_z}{L_{z,0}} \tag{7}$$

A comparison between $\lambda_{z,m1}$, $\lambda_{z,m2}$, and $\lambda_{z,M}$ provides an indication of the extent that the affine model accurately describes the deformation.

2.3. Chain Segment Orientation. We have also investigated the orientation correlation, $S(r)$, of elastic chains and probe chains that are trapped in the network. Local segment correlations are not directly observable by experiments but can be calculated directly using simulation. We used a method for calculating an orientation correlation developed by Yong and Higgs,[15] except that they calculate $S(r)$ with respect to all monomers within a separation distance r, whereas in our work we are interested in the orientation correlation between monomers of the same chain.

Use of this method is illustrated by a diagram of a 7-mer shown in Figure 2, where all the monomers are considered to be in the same xy plane for simplicity. The direction of the chain at any given monomer, except the end monomers, is defined as the sum of the two bond vectors that meet at that monomer. The direction of the chain at any given monomer can also be considered to be the tangent to the polymer at the monomer. Examples of these "tangent" vectors are shown in Figure 2. Here, **u** is the tangent vector at monomer 2, and $\mathbf{v_1}$ and $\mathbf{v_2}$ are tangent vectors at monomer 5 and 6, respectively. The angle $\gamma_{\mathbf{uv}}$ is calculated between **u** and $\mathbf{v_1}$ or $\mathbf{v_2}$ depending on the distance r between them. The extent of orientation correlation can then be expressed by[15]

$$S(r) = \frac{\sum P_2(\cos\gamma_{\mathbf{u,v}})}{N_r} \tag{8}$$

where P_2 is the second Legendre polynomial and N_r is the number of pairs of monomers that have separation r. The distance r is measured in number of lattice constants. The sum is over all pairs of monomers within each chain that have separation r in an instantaneous configuration. In determining the monomers that have separation r, the two end monomers of a chain must be excluded. A value of the orientation correlation of unity, $S(r) = 1$, indicates complete parallel alignment, while $S(r) = -1/2$ indicates perpendicular alignment, and $S(r) = 0$ indicates random orientation of segments.

2.4. Characteristics of the Polymer Systems. We studied systems of athermal 10-mers and 50-mers in the framework of the three-dimensional bond fluctuation model.[24,25] All simulations of the 10-mer systems had 1225 chains and were performed on a $60 \times 60 \times 60$ lattice, and all simulations of the 50-mers had 968 chains and were performed on a $95 \times 95 \times 95$ lattice. Periodic boundary conditions were imposed in the x and y dimensions, and hard walls were placed in the z dimension to allow for the deformation simulations. The initial configuration was created by randomly inserting precursor polymer chains and cross-links in the simulation cell until melt density conditions were reached. These linear chain systems were subjected to an isotropic osmotic pressure at the time of formation, and the empty lattice sites were considered to be solvent. The system was then equilibrated using monomer and cross-link displacement moves. During the equilibration phase, no reaction was allowed to occur. When the cure was started, a bond was allowed to form when an unsaturated chain end or cross-link moved into one of each other's six nearest-neighbor positions. The cure was stopped after the network imperfections and soluble fraction ceased changing significantly. Both the 10- and 50-mer networks had minimal soluble material (less than 0.5%). The networks that were created had a stoichiometric ratio of cross-link sites to chain ends. Also, to perform a study of the chain segment orientation of free linear probe chains trapped in polymer networks, 10 unreactive 50-mer linear probe chains were included with the 50-mer precursor chains that were allowed to cure into 50-mer networks. Additional details of the methodology of network formation can be found elsewhere.[30,31] Since these networks were formed with a hard wall the z direction, the initial configurations of the polymer melt and the resulting network deviate slightly (less than 10%) from Gaussian behavior. This effect is not expected to affect the conclusions presented in this paper.

Table 1. Network Properties as a Function of Osmotic Pressure for the 10-mer Networks

π^*	$\langle\phi\rangle$	$\langle R_{e,xy}^2\rangle/\langle R_{g,xy}^2\rangle$	$\langle R_{e,z}^2\rangle/\langle R_{g,z}^2\rangle$	$\lambda_{z,m1}$	$\lambda_{z,m2}$	$\lambda_{z,M}$
0.00	0.215 ± 0.011	6.05 ± 0.04	7.84 ± 0.09	1.74 ± 0.03	1.67 ± 0.01	~2.10
0.02	0.318 ± 0.003	5.86 ± 0.07	6.63 ± 0.04	1.27 ± 0.01	1.25 ± 0.01	1.65
0.04	0.394 ± 0.003	5.85 ± 0.04	6.10 ± 0.11	1.10 ± 0.01	1.10 ± 0.03	1.33
0.06	0.447 ± 0.003	5.83 ± 0.05	5.84 ± 0.10	1.02 ± 0.01	1.04 ± 0.05	1.12
0.10	0.529 ± 0.004	5.81 ± 0.06	5.48 ± 0.04	0.92 ± 0.01	0.95 ± 0.06	0.85

Table 2. Network Properties as a Function of Osmotic Pressure for the 50-mer Networks

π^*	$\langle\phi\rangle$	$\langle R_{e,xy}^2\rangle/\langle R_{g,xy}^2\rangle$	$\langle R_{e,z}^2\rangle/\langle R_{g,z}^2\rangle$	$\lambda_{z,m1}$	$\lambda_{z,m2}$	$\lambda_{z,M}$
0.00	0.154 ± 0.010	6.16 ± 0.11	9.13 ± 0.10	2.47 ± 0.06	2.55 ± 0.02	~2.56
0.01	0.249 ± 0.002	6.00 ± 0.06	7.32 ± 0.11	1.49 ± 0.01	1.59 ± 0.01	1.97
0.02	0.314 ± 0.002	6.09 ± 0.08	6.73 ± 0.10	1.25 ± 0.01	1.35 ± 0.01	1.55
0.04	0.394 ± 0.001	6.11 ± 0.09	6.00 ± 0.07	1.03 ± 0.01	1.11 ± 0.01	1.20
0.06	0.446 ± 0.001	6.12 ± 0.07	5.76 ± 0.10	0.94 ± 0.01	1.03 ± 0.01	0.99
0.08	0.482 ± 0.002	6.25 ± 0.06	5.53 ± 0.22	0.89 ± 0.01	0.98 ± 0.02	0.93
0.10	0.518 ± 0.001	6.23 ± 0.10	5.24 ± 0.16	0.82 ± 0.01	0.90 ± 0.01	0.91

3. Results and Discussion

3.1. Osmotic Pressure Dependence on Concentration. Osmotic pressure vs concentration data for 10-mer and 50-mer athermal networks were determined by varying the osmotic pressure, π^*, using the new NpT methodology presented above. The polymer networks were allowed to uniaxially swell (network absorbed empty lattice sites) or deswell (network exuded empty lattice sites) with a range of positive osmotic pressures. Swelling occurs when π^* is set smaller than the π^* of formation, and deswelling occurs when π^* is greater than the π^* of formation. The two-layer purely repulsive potential described above was used with $S = 80$ steps for all simulations of networks that were performed at positive osmotic pressures. Additionally, the networks were swollen to equilibrium by setting the osmotic pressure to zero. In the zero pressure simulations, the 20-step, 7-layer potential shown in Figure 1 was used.

In Figures 3 and 4, the profiles of the volume fraction in the z direction of the deformed networks are shown. As is expected, the volume fraction decreases as the osmotic pressure decreases. The bulk volume fraction is taken as the volume fraction where the profile is flat. Similarly, the length of the sample in the z direction, L_z, is determined from the region where the profile is flat. As the figures show, the wall effects extend less than 10 lattice layers for the networks at positive π^*, leaving a large number of layers within the bulk region. At $\pi^* = 0$, however, the profiles indicate that wall effects extend considerably farther than for the profiles for $\pi^* > 0$. These effects are attributed to the high degree of swelling that the networks experience at $\pi^* = 0$. The peaks of slightly increased volume fraction at the edges of the profile of the 10-mer network at $\pi^* = 0$ are an artifact of the attractive potential at the wall. While the attractive component in the wall−polymer potential was chosen such that it was sufficient to anchor the edges of the network to the walls at $\pi^* = 0$, the specific threshold at which the attractive part of the potential becomes strong enough to anchor the network to the walls was not determined. The bulk volume fractions for each osmotic pressure determined from Figures 3 and 4 are reported in Table 1 for the 10-mer networks and in Table 2 for the 50-mer networks.

The π^* vs $\langle\phi\rangle$ data of athermal 10- and 50-mer linear chains were determined using the same methodology as used in determining the network data. The two-layer wall−polymer potential was used for both linear chain sizes. For the system of linear 50-mer chains, $S = 80$ was used to determine the second layer of the wall−polymer potential. For the 10-mer linear chains, $S = 20$ was used for the system with the lowest pressure ($\pi^* = 0.0033$) and $S = 40$ was used for all other pressures. The profiles of the volume fraction in the z direction was flat with minimal wall effects as was observed with the networks with $\pi^* > 0$.

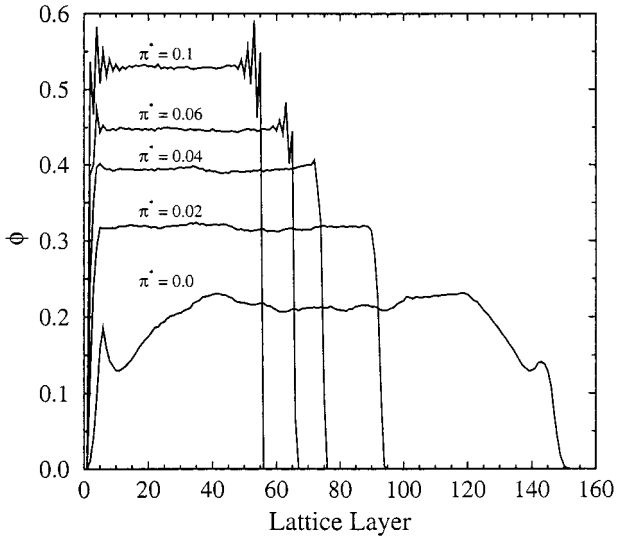

Figure 3. Profile of the volume fraction in the z direction for various osmotic pressures for an athermal 10-mer network.

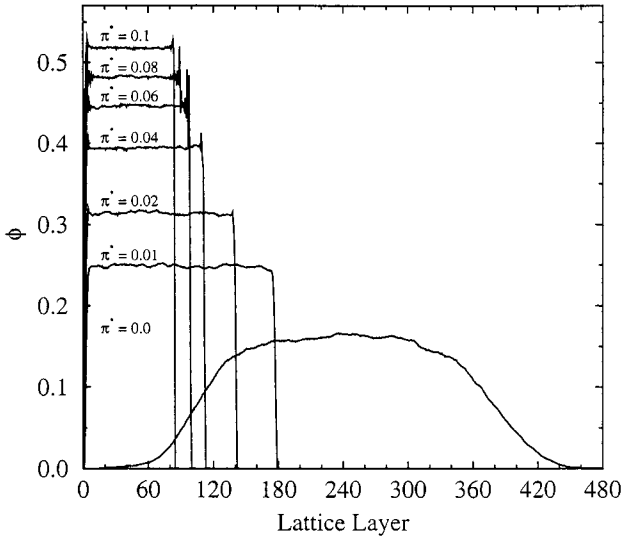

Figure 4. Profile of the volume fraction in the z direction for various osmotic pressures for an athermal 50-mer network.

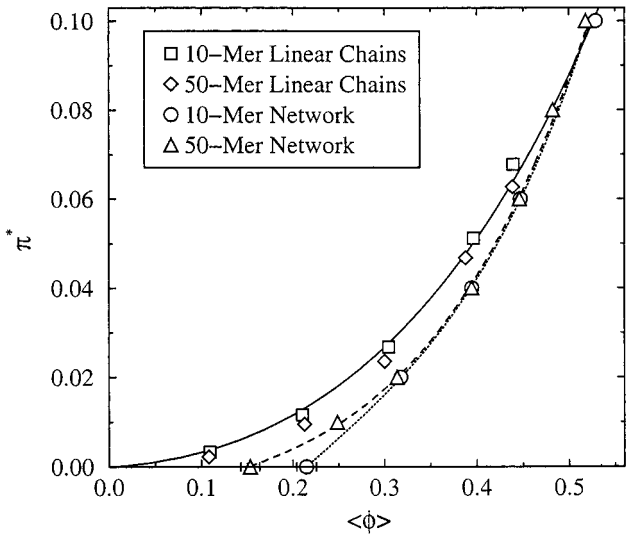

Figure 5. Osmotic pressure vs concentration for athermal 10- and 50-mer networks and linear chains. The solid line is the generalized Flory EOS,[32] and the broken lines are guides for the eye.

The π^* vs $\langle\phi\rangle$ data of the athermal 10- and 50-mer networks are presented in Figure 5 and compared with the athermal 10- and 50-mer linear chain data and the generalized Flory equation of state (EOS)[32] for a 10-mer athermal chain. The generalized Flory EOS is not shown for a 50-mer linear chain for visual clarity.

The simulation data for the 10-mer linear chains are in good agreement with the generalized Flory EOS at low to medium pressures. Although not shown, the 50-mer linear chains results are also in good agreement with the theory for 50-mer linear chains at low to medium pressures. Additionally, results from the 10- and 50-mer linear chain simulations appear to be somewhat similar. This is in agreement with previous simulations performed by Müller and Paul[33] that indicate that the osmotic pressure is nearly independent of the chain length. At high pressures, however, the simulation data of the linear chains underestimate the volume fraction calculated from the generalized Flory EOS. The same observation was made by Deutsch and Dickman,[32] who performed constant *NVT* Monte Carlo simulations of 10- and 20-mer athermal linear chains. They attribute the discrepancy between the pressure predicted by simulations and that obtained from the generalized Flory EOS to the prohibition of bonds of length $\sqrt{8}$ in the BFM. This is expected to introduce an additional hard core repulsion of 12 excluded neighbors between pairs of monomers. This effect is expected to yield an increased pressure (or a decreased volume fraction) and be of significance at higher densities.

Also, good agreement is observed in Figure 5 at high volume fractions between the simulation results for the networks and the generalized Flory EOS for 10-mer linear chains. In addition, the 10-mer and 50-mer network data are almost identical at high volume fractions. At low volume fractions, however, the network data deviate from the linear chain data and approach a region where negative pressures need to be imposed in order to continue the data to lower volume fractions. Similar results have been reported in the recent work of Escobedo and de Pablo[23] and Kenkare et al.[20]

The 10-mer network data in Figure 5 approach $\pi^* = 0$ with a steeper slope than the 50-mer data because the cross-link density (and consequently the modulus) of the 10-mer network is higher than that of the 50-mer network. If π^* vs $\langle\phi\rangle$ data are collected for networks formed with longer precursor chain lengths than 50-mer, the following effect is expected to occur. The 50-mer chain length is greater than the entanglement length, N_e ($N_e \approx 38$ for the BFM[25,18]), of the polymer melt. Molecular dynamics simulations performed by Duering et al.[34] indicate that when the precursor chain length becomes much greater than N_e, the modulus becomes independent of the cross-link density. Therefore, if the precursor chain length of the network is increased well beyond 50-mer, the modulus is expected to change very little and reach a plateau. Consequently, the π^* vs $\langle\phi\rangle$ data of a network formed with longer precursor chains are expected to roughly fall on a limiting asymptotic curve not too far from the 50-mer network curve.

3.2. Conformational Properties of the Elastic Chains. In Tables 1 and 2, the conformational properties of elastic chains in the 10-mer and 50-mer athermal networks are presented. In each table, the ratio of the mean-squared end-to-end distance in the direction of deformation, $\langle R_{e,z}^2\rangle$, to the mean-squared radius of gyration, $\langle R_{g,z}^2\rangle$, is compared to the ratio of the same properties perpendicular to the direction of deformation, $\langle R_{e,xy}^2\rangle$ and $\langle R_{g,xy}^2\rangle$. Additionally, values for the microscopic deformation ratios ($\lambda_{z,m1}$ and $\lambda_{z,m2}$) given by eqs 5 and 6 and the macroscopic deformation ratio $\lambda_{z,M}$ determined from eq 7 are reported.

The value of $\langle R_{e,xy}^2\rangle/\langle R_{g,xy}^2\rangle$ for both the 10- and 50-mer networks is approximately equivalent to 6, indicating that the chains are behaving in a Gaussian manner in the transverse directions x and y. On the other hand, the value of $\langle R_{e,z}^2\rangle/\langle R_{g,z}^2\rangle$ deviates significantly from 6 at low osmotic pressures, and this deviation is most pronounced for the 50-mer networks. This result suggests that the chain ends of the elastic chains deform to a greater extent than the internal segments of the chain and that this behavior is accentuated for the longer chains.

The results listed in Tables 1 and 2 indicate that while most of the values of $\lambda_{z,m1}$ and $\lambda_{z,m2}$ for both series of networks are not statistically identical, their values do not deviate by more than 10% for any osmotic pressure. It thus appears that the molecular deformation can be estimated reasonably well from the unperturbed molecular size, assuming affine deformation. On the other hand, large discrepancies are seen between the microscopic and macroscopic deformation ratios, particularly at low osmotic pressures or high deformation. This trend is apparent in the data in Tables 1 and 2, except at $\pi^* = 0$ for the 50-mer networks where $\lambda_{z,m} \approx \lambda_{z,M}$. This datum point is subject to significant uncertainties since it is somewhat ambiguous to determine L_z at $\pi^* = 0$ because wall effects extend considerably into the lattice as shown in Figure 4. Comparison between Figures 3 and 4 shows this uncertainty to be greater for the 50-mer networks.

3.3. Chain Segment Orientation. The orientation correlation was determined for monomer segments within trapped linear probe chains in the network and elastic network chains with respect to other monomer segments within the same chain using the procedure described in section 2.3. The correlation $S(r)$ was determined for 10 50-mer probe chains trapped in a 50-mer network. The results of the simulations reported here are for a system with hard walls in the x and y

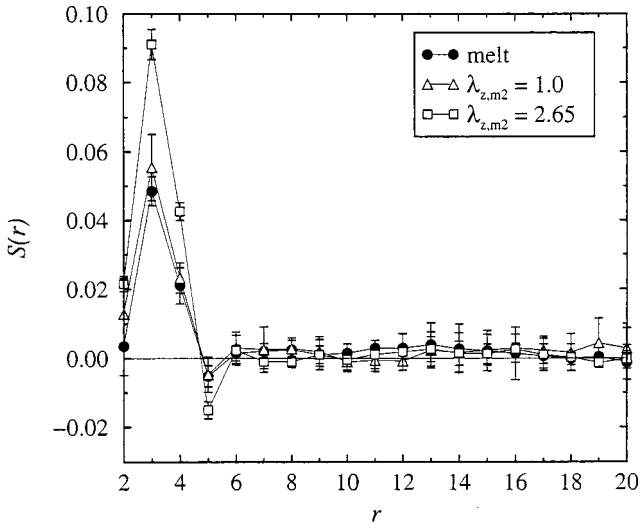

Figure 6. Orientation correlation, $S(r)$, of free linear probe chain segments with other segments of the same chain. $S(r)$ is for 50-mer probe chains in a 50-mer network. r is measured in number of lattice constants.

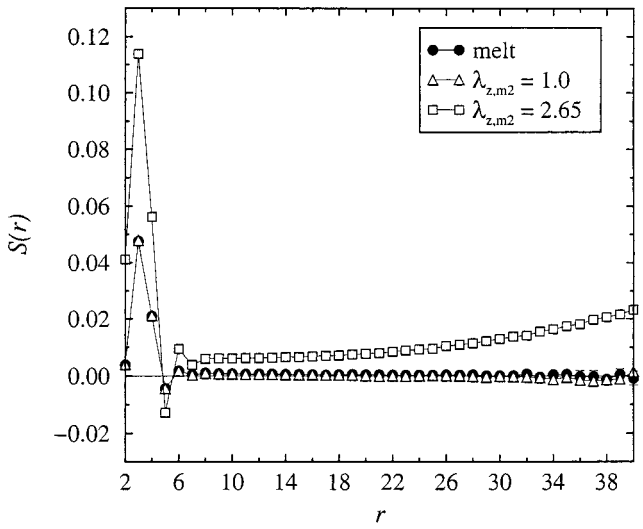

Figure 7. Orientation correlation, $S(r)$, of elastic chain segments with other segments of the same chain. $S(r)$ is for elastic chains in a 50-mer network. r is measured in number of lattice constants.

directions instead of periodic boundaries as presented in the rest of this study. Since the deformation is in the z direction, the calculation of $S(r)$ is not expected to be affected.

The correlation $S(r)$ as a function of separation distance r between monomers is shown in Figure 6. The variable used to describe the deformation is the microscopic deformation ratio $\lambda_{z,m2}$ presented in eq 6. Results are shown in Figure 6 for probe chains trapped in an undeformed network ($\lambda_{z,m2} = 1$) and a network that was swollen to equilibrium with $\pi^* = 0$ ($\lambda_{z,m2} = 2.65$). A solid line is drawn at $S(r) = 0$ as a reference. These results are compared to $S(r)$ of the probe chains in the melt prior to the cure. The plot shows that $S(r)$ of the free chains in the undeformed network and the melt are the same within the statistical uncertainty. There is a peak in the orientation at $r = 3$, a small negative correlation at $r = 5$, and then no discernible correlation for $r > 5$. The peak occurs at $r = 3$ because the probe chain is highly kinked in such a manner that the tangent vector at any given monomer is more oriented with respect to the tangent vector of a neighbor three lattice spacings away, rather than two lattice spacings. The small negative correlation at $r = 5$ is hypothesized to occur as a response to the positive correlation observed at lower r values.

$S(r)$ of the free chains in the deformed network shows higher positive orientation correlation for $r < 5$ and a stronger negative orientation correlation for $r = 5$. For $r > 5$, however, the probe chains behave the same as in the melt and the isotropic network and display no orientational preference. Thus, these simulation results indicate that deformation induces intrapolymer alignment of probe polymers at short distances, while maintaining no preferential order at larger distances. This result corroborates the suggestion of Boué et al.[9] that probe chains exhibit alignment at short length scales, while remaining unperturbed at large length scales.

Additionally, $S(r)$ of elastic chains in both undeformed and deformed networks was determined and is shown in Figure 7. Again, $S(r)$ of the elastic chains in an undeformed network is identical to $S(r)$ of the precursor chains in the melt for all distances. At small distances, the qualitative behavior of $S(r)$ of the elastic chains in the deformed network is identical to the behavior of $S(r)$ of the free chains in the deformed network. Quantitatively, however, $S(r)$ of the elastic chains has a slightly higher value at $r < 5$. At larger distances, however, $S(r)$ of the elastic chains does not return to a random orientation as the free chains do, but instead maintains a positive correlation. This behavior is expected since the elastic chains become more aligned during uniaxial deformation as has also been reported elsewhere.[15] In addition, the positive correlation increases in a nonlinear manner with increasing distance between the segments of an elastic chain. This result suggests that the orientation of chain segments at one end of a network chain are more strongly correlated with the orientation of the segments at the other end of the chain than with the orientation of segments at the center of the chain. The chain ends appear to deform to higher extents than the internal chain segments. This observation is consistent with the results presented above that indicate non-Gaussian behavior of elastic chains at large deformation.

4. Conclusions

Deformation of end-linked polymer networks was studied by Monte Carlo simulations using the athermal, three-dimensional bond fluctuation model. A novel methodology was presented that allows for volume change moves on a lattice in the constant NpT ensemble while maintaining the dynamical behavior and structural characteristics of the polymer network during deformation. This methodology was applied to determine the $P-V$ behavior of athermal 10- and 50-mer polymer networks and the $P-V$ behavior of 10- and 50-mer linear chains. Minimal wall effects were observed for the linear chain systems. The networks were allowed to uniaxially swell and deswell under a range of positive osmotic pressures. Minimal wall effects were present at nonzero osmotic pressures. The networks were also allowed to uniaxially swell to equilibrium using zero pressure simulations. A multilayer, multistep potential was used to perform the volume change in increments. The concentration dependence of the osmotic pressure of the linear chain and network systems were compared

with the generalized Flory EOS. For the linear chains, the results were found to be in excellent agreement with the generalized Flory EOS at low pressures and deviated slightly at high pressures as previously observed.[32] Also, at high volume fractions, the results for the athermal networks coincided with those of the linear polymer chains, but they deviated at lower volume fractions.

The conformational properties of the elastic chains of a network were investigated. The chain dimensions in the direction of deformation were found to be highly non-Gaussian for large deformations, while the chain dimensions in the directions perpendicular to deformation remained approximately Gaussian. This effect is believed to be a consequence of greater extension of the chain ends compared to extension of internal chain segments.

Segment orientation correlations within elastic and probe chains were calculated for chains in networks before and after deformation. Increased orientation correlations were found at small distances for both the elastic network chains and trapped linear probe chains in a strained network. At larger distances, the linear probe chains displayed no orientational preference. Additionally, increased orientation correlation was present for the elastic network chains in the deformed network at large distances, and the correlation increased with increasing separation distance. This result indicates that the elastic chains were not deformed homogeneously and suggests that segments near the chain ends were more aligned than internal segments.

Acknowledgment. Financial support for this work was provided by the Polymers Program of the National Science Foundation under Grants DMR-9706066 and 0078863.

References and Notes

(1) Mark, J. E.; Erman, B. *Rubberlike Elasticity: A Molecular Primer*; Wiley-Interscience: New York, 1988.
(2) Sotta, P.; Deloche, B.; Herz, J.; Lapp, A.; Durand, D.; Rabadeux, J.-C. Local order in monomodal and bimodal polymer networks: Monte Carlo simulations. *Macromolecules* **1987**, *20*, 2769−2774.
(3) Gronski, W.; Stadler, R.; Jacobi, M. M. Evidence of nonaffine and inhomogeneous deformation of network chains in strained rubber-elastic networks by deuterium magnetic resonance. *Macromolecules* **1984**, *17*, 741−748.
(4) Brereton, M. G. NMR study of the molecular anisotropy induced in a strained rubber network. *Macromolecules* **1993**, *26*, 1152−1157.
(5) Brereton, M. G.; Ries, M. E. An analytic study of the NMR properties for deformed polymer networks blended with free chains. *Macromolecules* **1996**, *29*, 2644−2651.
(6) Ylitalo, C. M.; Zawada, J. A.; Fuller, G. G.; Abetz, V.; Stadler, R. Oligomers as molecular probes of orientational coupling interactions in polymer melts and networks. *Polymer* **1992**, *33*, 2949−2960.
(7) McLoughlin, K.; Szeto, C.; Duncan, T. M.; Cohen, C. End-linked poly(dimethylsiloxane) elastomer structure: ^{2}H NMR transverse dephasing data compared to predictions of statistical and thermodynamic models. *Macromolecules* **1996**, *29*, 5475−5483.
(8) McLoughlin, K.; Waldbieser, J. K.; Cohen, C.; Duncan, T. M. End-linked poly(dimethylsiloxane) elastomers: ^{2}H−Nuclear magnetic resonance investigations of compression-induced segment anisotropy. *Macromolecules* **1997**, *30*, 1044−1052.
(9) Boué, F.; Farnoux, B.; Bastide, J.; Lapp, A.; Herz, J.; Picot, C. Free polymer chains dissolved in a strained elastomer: Neutron scattering test of the anisotropy. *Europhys. Lett.* **1986**, *12*, 637−645.
(10) Sotta, P. Local order in monomodal and bimodal polymer networks: Monte Carlo simulations. *Macromolecules* **1998**, *31*, 8417−8422.
(11) Depner, M.; Deloche, B.; Sotta, P. Uniaxiality induced in a strained polymer network: Theory and Monte Carlo simulations. *Macromolecules* **1994**, *27*, 5192−5199.
(12) Baljon, A. R. C.; Grest, G. S.; Witten, T. A. Simulations of induced orientation in stretched polymer melts. *Macromolecules* **1995**, *28*, 1835−1840.
(13) Gao, J.; Weiner, J. H. Chain force concept in systems of interacting chains. *Macromolecules* **1991**, *24*, 5179−5191.
(14) Sotta, P.; Higgs, P. G.; Depner, M.; Deloche, B. Monte Carlo simulations of the orientational order in a strained polymer network: Effect of density. *Macromolecules* **1995**, *28*, 7208−7214.
(15) Yong, C. W.; Higgs, P. G. Chain orientation in polymer networks: Computer simulations using the bond fluctuation model. *Macromolecules* **1999**, *32*, 5062−5071.
(16) Gao, J.; Weiner, J. H. Anisotropy effects on chain-chain interactions in stretched rubber. *Macromolecules* **1991**, *24*, 1519−1525.
(17) Sommer, J.-U. Structural properties and swelling behavior of randomly cross-linked polymer networks: A Monte Carlo study. *Macromol. Symp.* **1994**, *81*, 139−152.
(18) Trautenberg, H. L.; Sommer, J.-U.; Göritz, D. Structure and swelling of end-linked model networks. *J. Chem. Soc., Faraday Trans.* **1995**, *91*, 2649−2653.
(19) Hölzl, T.; Trautenberg, H. L.; Göritz, D. Monte Carlo simulations on polymer network deformation. *Phys. Rev. Lett.* **1997**, *79*, 2293−2296.
(20) Kenkare, N. R.; Hall, C. K.; Khan, S. A. Pressure−volume properties of endlinked hard-chain polymer networks. *J. Chem. Phys.* **1999**, *110*, 7556−7573.
(21) Escobedo, F. A.; de Pablo, J. Monte Carlo simulation of branched and cross-linked polymers. *J. Chem. Phys.* **1996**, *104*, 4788−4801.
(22) Escobedo, F. A.; de Pablo, J. Simulation and theory of the swelling of athermal gels. *J. Chem. Phys.* **1997**, *106*, 793−810.
(23) Escobedo, F. A.; de Pablo, J. Phase behaviour of model polymeric networks and gels. *Mol. Phys.* **1997**, *90*, 437−443.
(24) Deutsch, H.-P.; Binder, K. Interdiffusion and self-diffusion in polymer mixtures: A Monte Carlo study. *J. Chem. Phys.* **1991**, *94*, 2294−2304.
(25) Paul, W.; Binder, K.; Heermann, D. W.; Kremer, K. Crossover scaling in semidilute polymer solutions: A Monte Carlo test. *J. Phys. II* **1991**, *1*, 37−60.
(26) Pendzig, P.; Dieterich, W.; Nitzan, A. Constant pressure simulations of lattice gas models. *J. Chem. Phys.* **1997**, *106*, 3703−3709.
(27) Nies, E.; Cifra, P. Equation of state behavior and interfacial properties of lattice chain fluids: A comparison of lattice fluid theory and Monte Carlo simulation. *Macromolecules* **1994**, *27*, 6033−6039.
(28) Mackie, A. D.; Panagiotopoulos, A. Z. Monte Carlo simulations of phase equilibria for a lattice homopolymer model. *J. Chem. Phys.* **1995**, *102*, 1014−1023.
(29) Dickman, R. *Measuring Forces in Lattice Polymer Simulations*; Springer-Verlag: Berlin, 1998; Vol. 102.
(30) Gilra, N.; Cohen, C.; Panagiotopoulos, A. Z. A Monte Carlo study of the structural properties of end-linked polymer networks. *J. Chem. Phys.* **2000**, *112*, 6910−6916.
(31) Gilra, N.; Panagiotopoulos, A. Z.; Cohen, C., submitted to *J. Chem. Phys.*
(32) Deutsch, H.-P.; Dickman, R. Equation of state for athermal lattice chains in a 3*d* fluctuating bond model. *J. Chem. Phys.* **1990**, *93*, 8983−8990.
(33) Müller, M.; Paul, W. Measuring the chemical potential of polymer solutions and melts in computer simulations. *J. Chem. Phys.* **1994**, *100*, 719−724.
(34) Duering, E. R.; Kremer, K.; Grest, G. Structure and relaxation of end-linked polymer networks. *J. Chem. Phys.* **1994**, *101*, 8169−8192.

MA0021895